Journal Name

ARTICLE

Interactions of aggregating peptides probed by IR-UV action spectroscopy

Received 00th January 20xx,
Accepted 00th January 20xx

DOI: 10.1039/x0xx00000x

www.rsc.org/

Sjors Bakels,[a] Eline M. Meijer[a], Mart Greuell[a], Sebastiaan B.A. Porskamp[a], George Rouwhorst[a], Jerôme Mahé[b], Marie-Pierre Gaigeot[b] and Anouk M. Rijs [a,*]

Peptide aggregation, the self-assembly of peptides into structured beta-sheet fibril structures, is driven by a combination of intra- and intermolecular interactions. Here, the interplay between intramolecular and formed inter-sheet hydrogen bonds and the effect of dispersion interactions on the formation of neutral, isolated, peptide dimers is studied by infrared action spectroscopy. Therefore, four different homo- and hetereogeneous dimers formed from three different alanine-based model peptides have been studied under controlled and isolated conditions. The peptides differ from one another in the presence and location of a UV chromophore containing cap on either the C- or N-terminus. Conformations of the monomers of the peptides direct the final dimer structure: strongly hydrogen bonded or folded structures result in weakly bound dimers. Here the intramolecular hydrogen bonds are favored over new intermolecular hydrogen bond interactions. In contrast, linearly folded monomers are the ideal template to form parallel beta-sheet type structures. The weak intramolecular hydrogen bonds present in the linear monomers are replaced by the stronger inter-sheet hydrogen bond interactions. The influence of π-π disperion interactions on the structure of the dimer is minimal, the phenyl rings have the tendency to fold away from the peptide backbone to favour intermolecular hydrogen bond interactions. Quantum chemical calculations confirm our experimental observations.

Introduction

The aggregation or self-assembly of peptides or proteins from their soluble, native structure into insoluble beta-sheet rich amyloid aggregates is directly related to both biological function as well as human diseases.[1-7] To date over 45 proteins and peptides are known to form disease related amyloid fibrils.[5] This long list of amyloid diseases resulted in the toxic association of amyloid formation with the most well-known examples being Alzheimer's Disease and Parkinson's Disease. The current general consensus that the early-stage formed intermediate oligomers are the actual malefactors[8-10] and not the full-grown fibrils has resulted in the demand to understand the structure and interactions of these oligomer intermediates and the mechanism elucidating the early steps in peptide self-assembly. Most experiments aim to determine the structure of the full-grown fibrils or obtain an averaged picture of the ensemble of intermediate structures and morphologies.[7, 8, 11-14] Extensive studies based on structural techniques such as X-ray diffraction, electron microscopy and solid-state NMR have revealed high-resolution structural information on these final states, but information on earlier aggregation stages is hampered due the non-crystalline nature and the broad heterogeneity of the pre-fibrils. Spectroscopic methods such as circular dichroism and FTIR are able to provide such structural information, but the information gained solely represents an average of all the aggregation states.[15] It is thus impossible to obtain structural details over individual clustered peptide aggregates with these methods. Mass spectrometry combined with ion mobility has been very successful to study lowly populated species in heterogeneous mixtures and reveal how aggregates might evolve.[4, 16, 17] More recently, spectroscopic experiments are being developed that bring detailed structural insights of low populated species.[18-22] Electrospray ionization is generally used in combination with these advanced mass spectrometry methods to bring the peptide aggregates as charged species into the gas phase. It was shown that an increase in beta-sheet character, which is indicative for the regular aggregate structure, was observed in more extended oligomers where also the charge states played an important role. Studying peptide aggregation under neutral conditions might provide more insights into non-charge driven aggregation interactions such as dispersion interactions such as NH-π and π−π stacking, and intra- and intermolecular hydrogen bond interactions.[23-26] As for example, the π−π interactions are expected to play a directing role by stabilizing hydrophobic domains crucial for the development of amyloid structures. [24, 27-31]
Although cluster formation between (bio)molecules and solvent molecules such as water or methanol are rather straightforward by co-expanding the solvent molecules with the seed gas[32-35], the formation of aggregates of neutral peptides is not. Until

[a.] Radboud University, Institute for Molecules and Materials, FELIX Laboratory, Toernooiveld 7-c, 6525 ED Nijmegen, the Netherlands. E: a.rijs@science.ru.nl
[b.] LAMBE CNRS UMR8587, Universite´ d'Evry val d'Essonne, Blvd F. Mitterrand, Bât Maupertuis, 91025 Evry, France.
Electronic Supplementary Information (ESI) available: See DOI: 10.1039/x0xx00000x

recently, only a few examples were published where peptide dimer clusters were formed in the gas phase using laser desorption or thermal evaporation.[27, 31, 36, 37] Recently, we showed using laser desorption that the aggregation of overall neutral peptides is not limited to the formation of dimers anymore, but is brought into the regime of 10-15 peptides assembled together.[38] This allows us to study the onset of peptide oligomerization at molecular-level details.

Here, we aim to understand the intrinsic driving forces of peptide self-aggregation; i.e. probing the influence of intra- and inter-molecular interactions on the structure of formed peptide dimers. Therefore, we have studied three different aggregating model peptides where we incorporated a UV chromophore on either end of the peptide and a third one without any UV chromophore, see Fig.1. By comparing the experimentally present conformers for the monomeric peptides with the formed homogeneous and heterogeneous dimers and theoretical quantum chemical calculations, we can elucidate whether intramolecular hydrogen bonds of the bare monomeric conformer remain preserved or will be broken favouring new interactions upon dimerization. Moreover, the possible role of dispersion interactions can be probed by comparing the homogeneous and heterogeneous dimers, where the position of the phenyl ring is either altered or eliminated.

Z-Ala-Ala-OMe "A"

Ac-Ala-Ala-OBn "B"

Ac-Ala-Ala-Ala-OMe "3"

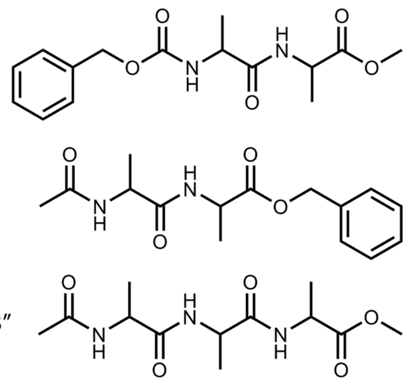

Figure 1: Chemical structures of the studied peptides a) Z-Ala-Ala-OMe (peptide A), b) Ac-Ala-Ala-OBn (peptide B), and Ac-Ala-Ala-Ala-OBn (peptide 3) forming the homogeneous dimers "AA" and "BB" and the heterogeneous dimers "AB" and "B3".

Methods

a. Experimental

A description of the laser desorption molecular beam set-up and experimental methods have been reported in great detail recently.[39, 40] Therefore, the experimental set-up is described only briefly by focusing on specific important parameters for the experiments presented here.

The peptide molecules studied in this work, Z-Ala-Ala-OMe, Ac-Ala-Ala-OBn, and Ac-Ala-Ala-Ala-OMe, were purchased from BioMatik (95% purity), and used without any further purification. These peptide molecules were mixed with carbon black and subsequently deposited on the surface of a graphite sample bar. This sample bar is placed via an airlock into the high vacuum (~10^{-8} mbar) source chamber just in front of the nozzle of a pulsed valve (0.5 mm ⌀, 10 Hz, Jordan). A low intensity (1 mJ/pulse) Nd:YAG laser (New Wave Research, Polaris II, 1064 nm, 10 Hz) is mildly focused on the surface of this sample bar, thereby desorbing the sample molecules from the graphite matrix. The sample bar is translated with a stepper motor to ensure that new sample is provided at each laser shot. After desorption the neutral gas phase molecules are directly cooled by the molecular beam of argon with a backing pressure of 3 bar. The dimers discussed in this work and higher order clusters are obtained using a larger distance between sample bar and nozzle opening than for monomeric peptides.[38] About 10 cm downstream, the neutral molecular beam passes a skimmer (2 mm ⌀), and enters the differentially pumped reflector-based time-of-flight mass spectrometer (Jordan Co.). The molecular beam is subsequently perpendicularly crossed with a UV and IR laser beam to perform spectroscopy. Ions created by resonant [1+1] photoionization were accelerated into the reflector time-of-flight tube and detected with a dual microchannel plate detector (Jordan Co.), yielding mass spectra with a resolution of M/ΔM of about 2000.[41]

The phenyl groups in peptide A and B (see Fig. 1) have a $\pi\pi^*$ transition around 266 nm and are used to resonantly excite them, and with a second photon, subsequently ionize the molecules in our experiment. This technique is conformer and multimer dependent, since every conformer and molecule have a different potential energy surface. IR absorption spectra were recorded using IR-UV ion dip spectroscopy (IR-IDS)[32] by spatially and temporally overlapping the IR and UV laser, where the IR laser arrives about 500 ns prior to the UV laser beam. The UV laser was fixed at a resonant wavelength, while the IR laser is scanned. When the IR laser is resonant with a vibrational transition of the studied peptide or peptide cluster, population is transferred from the ground state to a vibrational level, resulting in a depletion of the ground state population. This will create a dip in the ion signal created by the UV laser as the number of produced ions is reduced. By measuring the ion yield of the mass of interest while scanning the IR laser wavelength, a mass- and conformer selected IR ion-dip spectrum is recorded.

The IR spectra were recorded in the region between 1000 and 1800 cm^{-1}. This infrared light was provided by the Free Electron Laser FELIX.[42] FELIX produces pulses with a typical pulse duration of about 8-10 µs, pulse energies of about 100 mJ, and a spectral line width of about 0.5-1% of the IR frequency. IR on and off measurements were performed to correct for fluctuations in the signal, by running the experiment on 10 Hz (molecular beam, desorption and UV laser) and the IR laser on 5 Hz. Every measured point is an average of 30 shots with IR and 30 shots without IR. Absorbance spectra are obtained by taking the logarithm of the ratio between these two signals, dividing by the power of FELIX at each wavelength and multiplying by the photon energy in wavenumbers. For the monomeric peptides A and B the mid-IR spectra were recorded between 3000 and 3650 cm^{-1} produced by a YAG-pumped (Innolas Spitlight 600) OPO/OPA system (LaserVision).

b. Theoretical

Structural characterization relies on the comparison of the experimental IR spectra with the computed spectra resulting from quantum chemical calculations. First, a conformational search was performed using the amber force field.[43] Here, a starting structure of the peptide or peptide cluster was heated up to 300K for the dimers, and 1000K for the monomers. The structures were subsequently cooled down to 0K to find a minimum in the energy landscape and stored. This is repeated 500 times. Typically, about 500 structures were generated for each molecule, from which about 50 structures are selected based on their relative energy, chemical intuition and structural family. To sample the conformational landscape as complete as possible, multiple searches are performed, with different starting structures. All selected conformations were further optimized at the B3LYP-D3/6-31+G* level of theory for the dimers and B3LYP-D3/6-311+G** level of theory for the monomers and their vibrational frequencies were calculated using DFT in the Gaussian 09 environment. [44, 45] To correct for the anharmonicity a scaling factor of 0.976 was used for both the monomers in the infrared region between 1000 and 1800 cm^{-1}, while for the amide A infrared region a scaling factor was used of 0.955. For the dimers, the infrared region between 1000 and 1420 cm^{-1} and the amide I region were scaled with 0.976, while a mode dependent scaling factor of 0.962 was used in the dimers for the amide II modes (NH bending), the CH_2 bending and CH_3 umbrella and in and out of plane deforming modes between 1420 and 1600 cm^{-1}, as was discussed previously.[38] The zero-point energy (ZPE)-corrected energies and Gibbs free energies at 300 K are evaluated at the B3LYP-D3/6-31+G* level of theory.

Results

Peptide segments: In this work we focus on three alanine-based peptides. Previous studies have showed that alanine chains may favour the formation of beta-sheet dimers when they are clustered.[24] In order to study the role of stabilizing dispersion interactions and intra- and intermolecular hydrogen bond preferences, the peptides differ in the position of the UV tag position; i.e. (i) on the N terminal side for Z-Ala-Ala-OMe (peptide A) with a mass of 308 Da, (ii) on the C terminus Ac-Ala-Ala-OBn (peptide B) with a mass of 292 Da, and the third peptide Ac-Ala-Ala-Ala-OMe (peptide 3) with a mass of 287 Da has no UV chromophore. For peptide A and B their monomeric conformers have been identified using IR-UV ion dip spectroscopy, which is not possible for peptide 3 due to the absence of an UV chromophore. Subsequently, the IR spectra have been recorded for the homogeneous dimers AA and BB and heterogeneous dimers AB and B3.

Monomeric peptides A and B

Structure of Z-Ala-Ala-OMe (peptide A) monomer: The REMPI spectrum of Z-Ala-Ala-OMe is presented in Fig.SI.1 of the Supporting Information and shows two sets of features between 37300 and 37700 cm^{-1}, namely a slightly broadened peak around 37500 cm^{-1} and a set of sharp lines above 37550 cm^{-1}. IR-UV hole-burning experiments confirmed that they are originating from two separate conformations. Upon increasing the UV power to record the IR-UV ion dip spectra, a slight background appeared which originates from conformer A-II. In Fig.2 the experimental IR spectra of the two conformations are shown. A-I and A-II are obtained at an excitation wavelength of 37523 cm^{-1} and 37558 cm^{-1}, respectively.

Conformer A-I: The amide A region (N-H stretch, >3300 cm^{-1}) of the IR spectrum of conformer I of peptide A consists of two peaks at 3422 and 3480 cm^{-1}, see Fig. 2b (bottom panel). These frequencies typically correspond to a weakly hydrogen bonded NH moiety, for example an interaction with the π cloud of the phenyl group or a C5 interaction, and a free N-H stretch, respectively. By comparing the experimental IR spectra with our calculated IR spectra, we found in our calculations however, that the peak at 3480 cm^{-1} corresponds to the vibration of a C4 hydrogen bonded N-H and the peak at 3422 cm^{-1} indeed to a C5 interaction.

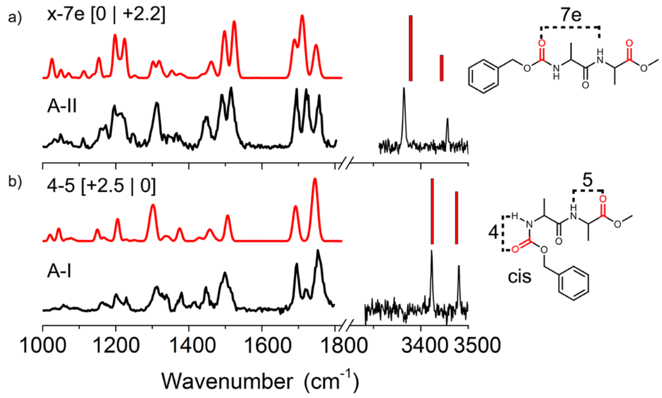

Figure 2: Experimental (black) infrared spectra of the two conformations of Z-Ala-Ala-OMe with a) conformer A-II and b) conformer A-I) both in the amide A (right panel) and mid-IR/fingerprint region (left panel). The red traces present the assigned calculated spectra with their respective structures given on the right, ester C=O groups indicated in red. The energetics are shown between brackets [zero-point energy | Gibbs free energy] both in kJ/mol.

The C=O stretching region comprises 3 C=O vibrations, two modes resulting from an ester group (O-C=O) of both end caps, which typically absorb between 1700 and 1770 cm^{-1}. The third C=O vibration results from a normal peptide bond C=O and has its absorption between 1600 and 1700 cm^{-1}. For these peptide bond C=O vibrations holds that a large red-shift coincided with a stronger hydrogen bond interaction. Two dominant peaks are observed in the experimental mid-IR spectrum of peptide A-I (left side of Fig. 2b) namely at 1696 and 1753 cm^{-1}. A third small peak is present at 1719 cm^{-1}. The most red located C=O peak at 1696 cm^{-1} indicates that the peptide C=O group is free, and thus not involved in any hydrogen bonding. The second peak at 1719 cm^{-1} is unexpected, since it suggests a very strong hydrogen bond of one of the ester C=O groups, while both NH peaks in the amide A indicate only weak hydrogen bonds. Finally, the peak at 1753 cm^{-1} is significantly broader than the other peaks that were measured in this region (23 cm^{-1} instead of typically 15 cm^{-1} at this wavelength region). These findings indicate that this last peak actually consists of two C=O vibrations, and that the peak at 1719 cm^{-1} originates from conformer A-II (see Fig 2a). The UV peak of conformer A-I was originally located on a broad band resulting from conformer A-II, although upon improved cooling this contribution disappeared, see Fig. SI.1. Therefore, we have to keep in mind that strong IR signatures of conformer A-II might be present in the IR spectrum of A-I. The calculated IR spectrum of the assigned C4-C5 conformer also shows two peaks around 1753 cm^{-1} indicating that both ester C=O groups at both end-caps at the C- and N-terminus are similarly weakly involved in hydrogen bonding.

Additionally, the IR spectra show other structural diagnostic features such as the amide II region represented by the broad band around 1499 cm^{-1}, which is most likely broadened on the blue side of the peak by the overlapping absorption of conformer A-II. The large peak at 1300 cm^{-1} originating from CH bending modes and the three backbone motion peaks around 1200 cm^{-1} confirm the assigned C4-C5 hydrogen bonded structure. The assigned structure has two weak hydrogen bonds making up a ring of 4 atoms and a second ring of 5 atoms, see right panel of Fig. 2b. It is important to notice that the N-terminal Z-cap C=O is in a *cis* configuration with respect to the NH group of the first alanine. Although natural peptide bonds are typically oriented in a *trans* configuration with the exception for proline, here the NH-C=O peptide bond resulting from a bond between the Z-cap and the first alanine residue, appear to prefers to be in the *cis* configuration. As this involves a non-natural peptide bond, both *cis* and *trans* configurations were included in the computational search for the non-functional peptide moieties. The C4-C5 *cis* structure is only 2.5 kJ/mol higher in energy than the lowest energy conformer, but has the lowest energy when taking into account the Gibbs Free Energies at 300K.

Conformer A-II: The experimental IR spectrum of conformer A-II presented in Fig. 2a shows two distinct peaks in the amide A region at 3364 and 3456 cm^{-1}, which are both red-shifted compared to the peaks for conformer A-I. This shift and their position indicate a strongly hydrogen bonded NH, corresponding to a C7 interaction, and probably a weakly hydrogen bonded NH such as a C5 or π-bonded interaction. Three distinctive peaks are present in the amide I, namely at 1695, 1721 and 1757 cm^{-1}, all with comparable intensities. Two peaks appeared at similar frequencies as was observed for the A-I conformer, indicating an analogue structural arrangement of these C=O groups. The peak at 1695 cm^{-1} indicates that the C=O in the centre of the peptide is not involved in hydrogen bonding, the same holds for the ester C=O group corresponding to the vibration at 1757 cm^{-1}. However, the 1721 cm^{-1} peak is representative of a very strong hydrogen bond of one of the two ester C=O groups at the termini. This is supported by the red shifted NH band in the amide II region. We have assigned this conformer to the x-7e structure, with the ester C=O at the N-terminus involved in a C7 hydrogen bond with the alanine side group on an equatorial position. The NH located close to the N-terminus is not involved in hydrogen bonding. However, this peak is still slightly red shifted compared to the corresponding weakly hydrogen bonded NH (C4) of conformer A-I. This slight red-shift is known to appear when an adjacent C=O group is involved in a strong hydrogen bond interaction, i.e. the so-called neighbouring effect.[46] The doublet observed at 1200 cm^{-1} originating from amide III motions coupled with CH vibrations is also in agreement with the calculated spectrum, thereby confirming our assigned structure. This x-7e structure has the overall lowest zero-point corrected energy, and has a slightly elevated energy at 300K with respect to the A-I conformer.

Structure of Ac-Ala-Ala-OBn (peptide B) monomer: The REMPI spectrum of Ac-Ala-Ala-OBn (see Fig. SI.2 of the SI) is measured between 37400 and 37750 cm^{-1} and shows three dominant peaks followed by a vibrational progression of the most intense peak at 37550 cm^{-1}. Two conformers were identified by using IR-UV hole-burning: a sharp line at an excitation energy of 37495 cm^{-1} was named conformer B-I, and a more intense, slightly broader band at 37551 cm^{-1} with vibrational progression conformer B-II. A third peak in between the two conformers at 37530 cm^{-1} was previously assigned to either a conformer similar to B-II kinetically trapped by argon, or a fragmented complex with argon.[47] The experimental IR spectra presented in Fig.3 are obtained at an excitation wavelength of 37495 cm^{-1} for conformer B-I (Fig.3b) and 37551 cm^{-1} for conformer B-II (Fig.3a).

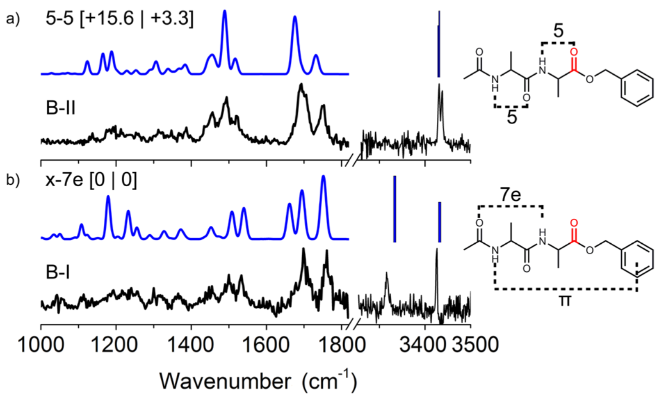

Figure 3: Experimental (black) IR spectra of conformer B-I and B-II of Ac-Ala-Ala-OBn (peptide B) measured in both in the mid-IR/fingerprint region (left panel) and the amide A region (right panel). The theoretical IR spectra (blue) of the assigned conformers are plotted above the experimental spectra with their respective structures drawn on the right. The energetics are shown between brackets [zero-point energy | Gibbs free energy], both in kJ/mol.

Conformer B-I and B-II: In a previous publication by the group of Mons et al. Ac-Ala-Ala-OBn was used as a model peptide to study the interplay between experiment probing the amide A region of the IR spectrum and theory.[47] They found two conformers present in their molecular beam experiments which were assigned by them to the lowest energetic structure (π-7e) and one lying 18 kJ/mol higher in energy (5-5). The π-7e structure, here conformer B-I, shows a C7 interaction between the ester C=O group of the acetyl-cap and the NH group of the second alanine residue, while the 5-5 conformer (here

Please do not adjust margins

conformer B-II) has two neighbouring C5 interactions, see right panel of Fig.3. The B-I conformer (5-5) is significantly higher in energy, however when including Gibbs Free Energies at around 330K this energy drops significantly. The higher energy conformer B-II is probably kinetically trapped, allowing us to observe it.[48, 49]

Fig.3 presents the experimental IR spectra of conformer B-I and B-II recorded in the mid-IR/fingerprint region from 1000-1800 cm^{-1}. For completeness, the amide A region was measured as well from 3250 to 3500 cm^{-1}. In this work, the functional B3LYP with the empirical dispersion D3 term from Grimme was used.[44] This functional gives similar results as B-97D as used in the paper by Mons et al.. In short, the assignments that were made by Mons et al. were confirmed by our work in the amide I, II and fingerprint infrared region.

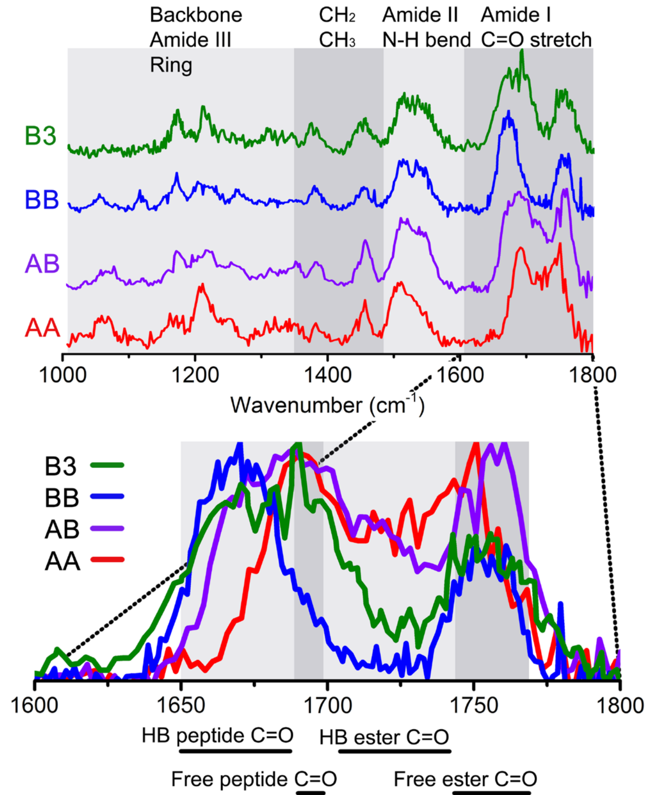

Figure 4: Top panel: Infrared spectra of all measured dimers, AA (red), AB (purple), BB (blue) and B3 (green) from bottom to top. The grey boxes indicate the vibrational modes in these regions. The bottom panel shows an enlargement of the amide I region, with the same colour coded spectra, but then on top of each other. Here, the spectrum is again divided into boxes, and below this figure a specification is given for the modes that can be found in these regions.

Dimer aggregates

To probe the role of hydrogen bond and dispersion interactions on the formation of beta-sheet dimers, the IR spectra of two homogenous dimers (AA and BB) and two heterogeneous dimers AB and B3 are measured. These dimers are expected to have different inter-strand and π–π interactions due to different ring and peptide moiety positions. The IR spectra and structure of both homogenous dimers of peptide A and peptide B are discussed in the next sections, followed by two heterogeneous dimers containing one A and one B peptide and a dimer containing peptide B and the non-chromophore containing peptide 3, respectively. Fig.4 shows an overview of the infrared spectra of these four measured dimers, along with indications of the origin of the observed vibrational modes. The inset shows a zoom in of the diagnostic amide I region.

Homogeneous dimer Z-Ala-Ala-OMe (AA): The REMPI spectrum of the dimer of peptide A (m/z= 616) shows a broad peak between 37430 and 37650 cm^{-1} (see red trace in Fig.SI.3). Infrared measurements were performed with the excitation laser fixed at 37480 cm^{-1}, which coincides with the red most feature in the REMPI spectrum. The obtained infrared spectrum is presented in the bottom trace of Fig.5 (black trace in Fig.5c). The spectra of the two conformers of monomer A are displayed above the spectrum of the dimer to compare the IR absorption of both monomers to the dimer. An average of their experimental spectra (in red) is plotted on top of the experimental spectrum of the AA dimer.

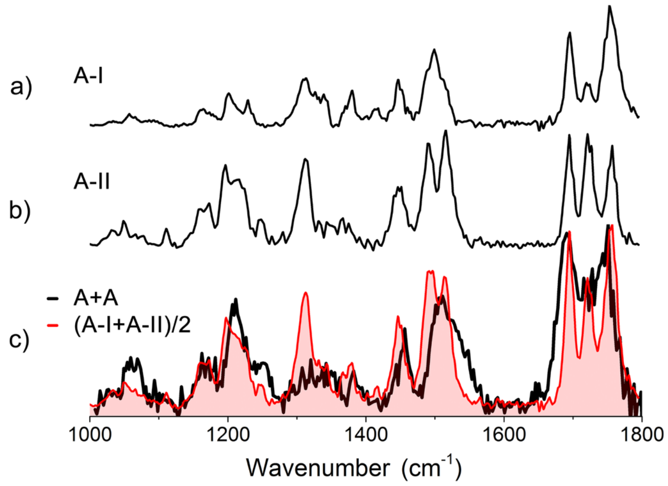

Figure 5: Experimental IR spectrum of a) conformer A-I and b) conformer A-II. c) the dimer of Z-Ala-Ala-OMe (peptide AA) in black compared to the averaged experimental spectra (in red) of both assigned conformers of the peptide A monomer.

The dimer AA has 6 C=O groups. Although each monomer has two amino acid residues, due to the presence of the ester caps, four ester C=O and only two peptide C=O groups are present, see Fig.1. The amide I region shows two dominant peaks for the AA dimer, with maxima at 1750 cm^{-1} and 1690 cm^{-1}, respectively (see Fig.5c). The latter peak is the most red shifted amide I peak, suggesting that none of the two peptide C=O groups are involved in hydrogen bonding. Two ester C=O moieties are likely weakly hydrogen bonded, while one ester C=O appears to be intramolecular hydrogen bonded and the last one intermolecularly. The amide II region shows a single broad peak at 1510 cm^{-1} with a shoulder slightly to the blue. No large shifts with respect to the individual monomer spectra are observed in both the amide I as the amide II region. Whereas the monomers both show a large peak around 1300 cm^{-1}, corresponding to C_α-H modes, the dimer does show a lower intense, broader feature. The three peaks at 1169, 1211 and 1248 cm^{-1} in the dimer spectrum are similar as the peaks observed in monomer A-II, and were there assigned to peaks involving motions of C_α-H coupled to amide III modes. Based on the comparison of the dimer IR spectra with the two averaged spectra of both conformers of the monomer, it appears that the dimer of peptide A is only weakly bound and the monomer structures are largely retained.

Quantum chemical calculations were performed in order to confirm this preliminary conclusion. 90 structures were found in multiple rounds of molecular dynamics simulations starting from different starting structures. Both parallel, anti-parallel and random structures were used as input structures, see Fig.SI.5b. When a parallel type structure was used as starting structure it always resulted in a range of different structures, except for a parallel type. For the other types, a family of structures similar to the original structure was present together with other structural families. The lowest energy structures were dominated by a mix of anti-parallel structures, a single hydrogen-bond parallel type and C8C8 structures (where a C16 ring was formed between the two monomers), see Fig. SI.5a. Above 10 kJ/mol with respect to the lowest energy structure, mainly structures were found where the two monomers were connected via a single hydrogen bond or via two hydrogen bonds in anti-parallel structures. Parallel structures almost exclusively appeared amongst the highest energetic structures. Due to the large amount of calculated IR spectra resulting from these 80 structures without an obvious match with our experimental IR spectrum, we designed the following approach: Every spectrum was evaluated by each diagnostic region (see Fig.4), and discarded when no agreement between experiment and theory was present. Firstly, we evaluated the amide I region, where we discarded around 40% of all structures. Secondly, the amide II region allowed us to remove an additional 28% of the structures, and finally 7% of all structures was eliminated based on the amide III of the spectrum. However, almost all calculations predict the amide III peaks too much to the higher energy side of the spectrum. Therefore, this 7% was based on relaxed criteria, and only structures were discarded when all the peaks were off for the amide III region. The calculated IR spectra of the final 10 structures with energies up to 30 kJ/mol are presented in Fig.SI.5c together with the four overall lowest energy structures per family and compared to the experimental spectrum in black. These calculated IR spectra include mostly low energy single hydrogen bonded structures, two anti-parallel structures with energies around +18 kJ/mol and a few high energy parallel structures (energies above 30kJ/mol). However, the average of the two monomers, as shown in Fig.5c (red trace), still provides a better match to the experimental spectrum than any of the calculated structures.

The primary conclusions to be drawn from the above findings are that the structure of the homogeneous dimer of peptide A probably originates from both conformers of the monomer A which are at most only weakly bound to each other by a single hydrogen bond. This is reflected by the minimal shifts of the amide I and amide II frequencies, but also in the preservation of the high intense peak in the conformationally important amide III region.

Homodimer Ac-Ala-Ala-OBn (BB): The experimental IR spectrum and the assignment of the Ac-Ala-Ala-OBn dimer (BB) is presented recently, therefore only a brief overview of the assignment is provided here.[38] The REMPI spectrum of the BB dimer (see Fig.SI.3) showed a broad feature which is red shifted with respect to the monomer. The peak is roughly 250 cm^{-1} broad and has its maximum absorption around 37518 cm^{-1}. The infrared spectra were predominantly recorded with a one photon energy of 37460 cm^{-1}, in order to measure the trimer and other higher order clusters at the same time. The infrared spectrum was also obtained at 37518 cm^{-1} which yielded the same IR spectrum indicating the presence of one dominant conformer, thereby justifying our chosen wavelength. Fig.6 shows the experimental infrared spectrum in black, showing two clearly distinctive peaks in the amide I region which correspond to the 2 ester C=O groups at 1753 cm^{-1} and the 4 peptide C=O vibrations grouped together at 1670 cm^{-1}. The experimental frequencies of the ester C=O peaks indicate that they are not involved in intermolecular hydrogen bonding. This is confirmed if we compare the weakly bound (C5) and free ester C=O groups in the both monomers which were observed at the same frequencies as those of the dimer.

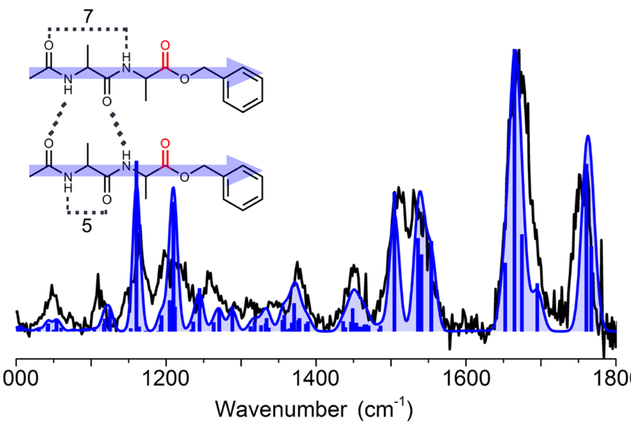

Figure 6: The experimental (black trace) spectrum of the dimer of Ac-Ala-Ala-OBn compared to the spectrum of the assigned calculated structure (blue trace). The inset shows the corresponding parallel type structure, the arrows pointing from the N-terminal side towards the C-terminus.

To assign the structure, an extensive conformational search was performed resulting in 80 different structures which were categorized into several structural families. These families were based on their respective hydrogen bond patterns (e.g. number of hydrogen bonds, (anti-)parallel beta-sheet pattern, and position of hydrogen bonds) as was similarly done for peptide dimer AA. Low lying energetic structures almost exclusively comprised beta-sheet structures with parallel type hydrogen bonds, whereas the first anti-parallel structure was over 20 kJ/mol higher in energy than the lowest energy structure (as shown in Fig. SI.6). The amide I region indicates that the two ester C=O groups were not involved in hydrogen bonding, while the 4 peptide C=O groups were all engaged in hydrogen bond interactions. This allowed us to exclude a high number of (higher energy) structural families and structures. Eight of the lowest energy structures per family are plotted in Fig.SI.6 for comparison. The remaining structural families were further examined, and based on the full spectrum between 1000 and 1800 cm^{-1} we assigned the structure to the overall lowest energy parallel beta-sheet type structure, see inset of Fig.6. The assigned structure is a combination of both monomer conformers, where the strong C7 intramolecular hydrogen bond of conformer B-II remained intact and only the weaker hydrogen bond (C5) in conformer B-I and the π-interaction in conformer B-II are broken to favour inter-strand hydrogen bonding.

Structure of heterogenous dimer of peptide A and B (AB): To create a dimer consisting of both peptide A and peptide B in our molecular beam set-up, peptide A and B were mixed in a 1:1 ratio and subsequently mixed with carbon black. The experiment was performed in a similar fashion as the homogeneous A and BB dimer aggregates. Since both molecules have a slightly different mass (A: 308 Dalton, B: 292 Dalton), the dimers AA, AB and BB were distinguishable in the mass spectrometer, see Fig.SI.4 of the SI. The REMPI spectrum of AB has a similar broad peak at the same UV excitation wavenumber as the AA and BB dimers; i.e. the rising edge is at the same position, but the peak ends in between the two other dimers (see Fig.SI.3). The excitation laser was fixed at 37490 cm^{-1} to obtain the IR-UV ion dip spectrum of the AB dimer as is shown in Fig.4 in purple. The mass-selected dimer AB consists of one monomer of A and one monomer of B. This means that we have in total six C=O groups of which three ester type C=O groups and three peptide-like C=O groups. The amide I region between 1600-1800 cm^{-1} shows two main bands: A main peak at 1757 cm^{-1}, and a peak at 1687 cm^{-1}, with a small shoulder at 1715 cm^{-1}. The first peak is in accordance with the C=O stretch vibration of a free ester C=O group, and is slightly blue shifted with respect to the peak of the AA dimer. The width of the peak indicates that most likely two ester type C=O groups are involved. The main peak has its maximum at 1688 cm^{-1}, which is more or less the same as the AA dimer (1691 cm^{-1}), and suggests free peptide C=O groups as we observed for the AA dimer. However, the band is broadened towards the red with respect to the AA dimer and all conformers of the A and B monomers. This overlap with the BB dimer peptide C=O vibrations indicates that probably at least one peptide C=O group is involved in a strong intermolecular hydrogen bonding.
The shoulder at 1715 cm^{-1} cannot be from a peptide C=O absorption as it is too much blue shifted, and is therefore allocated to a strong hydrogen bonded ester C=O moiety. This is confirmed by the NH bend vibrational modes in the amide II region, which show a peak at 1513 cm^{-1} and at 1539 cm^{-1}. Moreover, the peak is more broadened towards the blue than was observed for both homogeneous dimer IR spectra indicating indeed strong intermolecular hydrogen bonds. The intensity of the blue side of the amide II peak suggest that it probably comprises two intermolecular hydrogen bonded NH bend vibrations. The peak at 1513 cm^{-1} has the same position as the C7 (intramolecular) hydrogen bonded NH bending mode as was observed for conformer A-II of the A monomer peptide. This suggests that we have both original intramolecular hydrogen bonds present preserved from the monomeric peptide structures involving NH/C=O moieties in C7 or C5 intramolecular hydrogen bonds, while at the same time two other NH/C=O pairs are involved in intermolecular hydrogen bonding.

We have performed an extensive conformational search, which resulted in about 125 structures. For this conformational search, we used both assigned conformers of peptide A, i.e. including structures with the C=O and N-H of the Z-cap in a *cis* position with respect to each other. The same approach was used as described above in detail for dimer AA. By excluding all calculated structures which have poor agreement with the amide I region, 62% of all structure were discarded. Another 10% was rejected due to poor agreement in the amide II region. From the remaining structures, mainly singly hydrogen bonded structures, a handful parallel and anti-parallel structures and a few low energy structures with different types of double hydrogen bonding (e.g. C7-C8, enclosing a ring of 15 atoms), the lowest energy structures were plotted in FigSI.7 in the SI.
None of the calculated structures have a sufficiently good agreement with the experimental spectrum in order to make a conclusive assignment. However, considering the first 15 low energy structures (up to about 15 kJ/mol) which are predominantly parallel type conformations, parallel structures are most likely to be present. This is confirmed when we compare the experimental IR spectra of the AA (red) and BB (blue) dimer with the AB dimer (purple), see Fig.4. The IR signatures of the AB dimer are very similar as the signatures for the BB dimer throughout the full IR range, suggesting a similar structural arrangement as the peptide BB dimer: i.e. a parallel type beta-sheet. Zooming in on the amide I region, similarities with both the AA dimer and BB dimer are observed. The AB dimer shows a clear peak at 1715 cm^{-1} located in between the free ester-type C=O modes centred at 1757 cm^{-1} and the peptide C=O vibrations. This peak coincides with the strongly intramolecular hydrogen bond interaction as was observed for conformer A-II as well. The peak of the AB dimer resulting from the peptide-type C=O groups peaks at about 1687 cm^{-1}, showing a combination of both AA dimer as BB dimer absorption where both C=O moieties are engaged in intermolecular hydrogen bonds, see left figure of Fig.SI.6 (parallel C12 structure). The energies and spectral signatures indicate that conformer A-II and conformer B-II form this parallel beta-sheet. It is not surprising that conformer A-I is not observed within the AB dimer, due to its strong intramolecular hydrogen bond interactions and folded structure.

Characterization of heterogeneous dimer B3: The REMPI spectrum of dimer B3 formed from the co-desorption of Ac-Ala-Ala-OBn (peptide B) and Ac-$(Ala)_3$-OMe (peptide 3), see Fig.SI.2 of the SI, showed a very similar broad peak as the homodimer BB, with its maximum around 37518 cm^{-1}. As explained previously for the BB dimer, we have measured the infrared spectra using a UV photon energy of 37460 and 37518 cm^{-1}. Both yielded the same IR spectrum, as was also observed for the BB dimer. The experimental infrared spectrum of the B3 dimer, presented by the black trace in Fig.7 (and the green trace in Fig.4), shows the same spectral features although they appear to be slightly broadened and noisier with respect to the BB dimer due to experimental difficulties. Compared to the chemical structure of peptide B, the non-chromophore containing peptide 3 has one more peptide C=O and NH group, but the same number of ester-type C=O moieties, see Fig.1. This is directly visible in the amide I region of the IR spectrum of the B3 dimer. The peak corresponding to the ester C=O is similar in intensity, width and position as the BB dimer. This indicates that the ester type C=O groups are free and not involved in any hydrogen bond interactions. The peak between 1600 and 1720 cm^{-1} shows the same behaviour as the BB dimer, however there is an additional broadening to the blue side, with the peak at 1692 cm^{-1}, see the blue and purple trace of Fig.4. This corresponds typically to a free peptide C=O moiety or weakly hydrogen bond (C5, π) interaction. Also, the amide II shows a similar peak shape as BB, but slightly broadened and with more intensity at 1525 cm^{-1}, which is around the same wavenumber as a C5 intramolecular hydrogen bond found in the monomers. The same holds for the diagnostic amide III and CH bending band between 1150 and 1250 cm^{-1}. The peaks between 1000 and 1150 cm^{-1} originate from ring vibrations of the OBn-cap of peptide B. The weaker intensity of this group of peaks can be explained by the structure of the B3 dimer, which contains only one OBn group sinstead of two for the BB dimer. All these findings indicate a parallel structure for the B3 dimer as was found for the BB dimer.

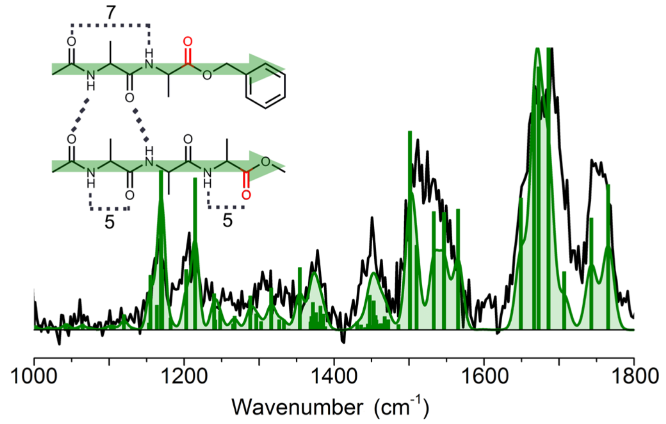

Figure 7: Experimental (black) and assigned calculated (green) infrared spectrum of the heterogeneous dimer B3. The inset shows the corresponding structure, which shows the same parallel intermolecular hydrogen bond pattern as the homogeneous dimer BB.

Quantum chemical calculations were used to substantiate these findings. Therefore, the 30 structures found in molecular dynamics simulations were optimized and their IR frequencies were calculated. As was observed before for the BB dimer, the lowest energy structures predominantly show parallel beta-sheet conformations, see Fig. SI.8. The first anti-parallel structure lies about 15 kJ/mol higher in energy than the lowest lying parallel structure. Other, more random structures such as C6-C6 interactions or C7-C11, also have reasonable energies (<20 kJ/mol). However, based on the amide I and amide II bands we could exclude the majority of the structures. Together with the lowest energy structures for each family this resulted in eight structures which are presented in Fig.SI.8 of the supporting information. We assigned the structure to a parallel C12 intermolecular hydrogen bond as indicated by the inset of Fig.7, although the other conformations with this similar parallel C12 interaction cannot be fully excluded. The assigned structure is analogue to the structure observed for the BB dimer.

Discussion

The structure of dimer BB is assigned to form a parallel type beta-sheet structure, where the inter-strand hydrogen bonds form a C12 ring, see Fig. 8. The dimerization into a parallel structure are by far the most stable structures that are found for the BB dimer (see Fig. SI.6a). The two monomers of which this dimer is formed originate both from the original conformers found in our experiment. Conformer B-I formed a strong C7 (gamma turn) intramolecular hydrogen bond, which has been preserved in the dimer structure. This C7 interaction slightly bends the backbone, thereby increasing the distance of the NH and C=O moieties of the first alanine residue such that these are in optimal position to form an inter-sheet hydrogen bond with conformer B-II. As can be seen from Fig.8 the two UV chromophores are pointing in the same direction in this parallel beta-sheet BB dimer. However, the phenyl rings do not engage in any π–π interaction and are folded away from each other.

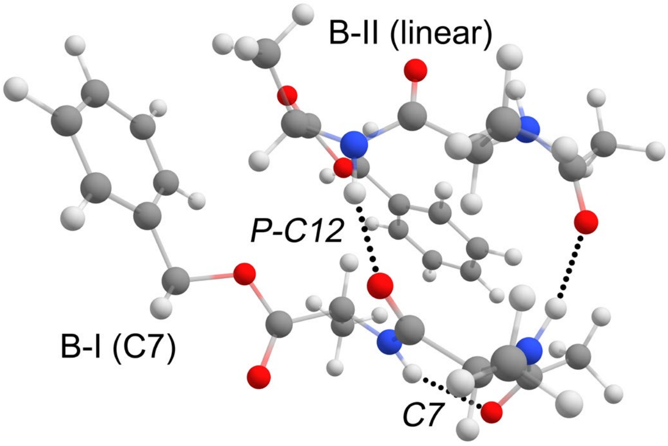

Figure 8: 3D visualization of the assigned structure of peptide BB. The ring of the top peptide (B-II) is folded away such that it does not interact with the ring of the C7 intramolecularly hydrogen bonded B-I peptide.

The heterogeneous B3 dimer shows the same parallel type structure as the BB dimer. The lowest energy structure of the BB dimer results from peptide B in the B-I conformation forming a C7 intramolecular hydrogen bond and the linearly structured peptide 3, which nucleates well on the template formed by the peptide B-I conformer (see Fig. SI.8). A similar result was previously observed for the Ac-Val-Tyr-Me and Ac-Ala_3-OMe dimer.[24] However, the reversed parallel structure, with peptide 3 in the C7 conformation and peptide B in the B-II conformation, is 2 kJ/mol higher in energy and shows only a slightly poorer agreement with the experimental spectrum, and cannot be excluded. Since peptide 3 does not contain a UV chromophore, its IR-UV ion-dip spectrum could not be recorded. Studying the infrared spectrum of peptide 3 using VUV ionization coupled to IRMPD might provide the required insight into the structure of the peptide monomer.[50] Since the same structure is formed for dimer BB and B3, we can conclude that the intermolecular π–π interaction does not play a significant role in the aggregation of these peptides.

In contrast, the AA dimer does not seem to form any beta-sheet structures, i.e. the AA dimer appears to be only weakly bonded. The IR spectra of all dimers indicate that the monomeric conformers are retained in their dimers and dictate the observed structure. The observed monomers of peptide A both have strong intramolecular hydrogen bonds resulting in a compact *cis* conformer and a C7 gamma turn conformer. The later would be an ideal platform to start the self-assembly when linear-type conformers would be present with weak intramolecular hydrogen bonds as we observed for the B3 and BB dimers.

In coincidence with the BB and B3 dimer, also the dimer of peptide AB was assigned to a parallel beta-sheet type structure. Similar IR spectral signatures are found for the AB, B3 and BB dimer. Additionally, the IR spectrum of the AB dimer shows the diagnostic peak of the preserved intramolecular C7 hydrogen bond signature of conformer A-II of peptide A. These findings are substantiated by the large presence of parallel type structures in the low energy structures of the molecular dynamics search. However, where we observe that in the dimers of BB and B3 a linear conformer (either conformer B-II or a linear conformer of 3) is used as template where a C7 intramolecular hydrogen bonded structure nucleates onto, in peptide AB only the B-II conformer has a linear structure. This limits the possible combinations to a cluster of conformer B-II (linear with C5-C5 hydrogen bonds) with conformer A-II (C7 gamma turn) to form a parallel C12 structure. The dominance of this dimer structure is expected, as this linear conformation is required to form higher order aggregates which we observed for all clusters as can be seen in Fig. SI.4.

Conclusions

The mass- and conformer-selective infrared spectra of four alanine-based dimers have been studied to probe (i) their propensity to form the well-known beta-sheet structures related to peptide aggregation and fibril formation, (ii) key IR signatures for aggregation, (iii) the competition between intra- and intermolecular interactions, and (iv) the role of other actions such as dispersion upon peptide aggregation. The studied peptide dimers consist of homogenous and heterogeneous combinations of Z-Ala-Ala-OMe (A), Ac-Ala-Ala-OBn (B), and Ac-Ala-Ala-Ala-OMe (3). The first two peptides have a benzyl group either on the N-terminus (A) or the C-terminus (B), which is used as a UV chromophore in our IR-UV ion-dip experiments. The monomers of both peptide A and B show 2 different conformations. Peptide A forms an γ-turn conformation via an intramolecular hydrogen bond forming a ring enclosing 7 atoms and a surprising *cis* folded structure, while for peptide B a similar C7 γ-turn structure was found together with a linear C5-C5 conformation.

Upon dimerization, the two homogenous dimers AA and BB showed a different picture. For the dimer of peptide B the well-known beta sheet structure was observed in a parallel orientation. However, no beta-sheet structure was obtained for the AA dimer. Both monomer conformations of peptide A are engaged in either strong hydrogen bond interactions or multiple weaker interactions resulting into a folded structure. As a result, both structures do not provide a suitable template for peptide dimerization. The IR spectra of both heterogenous dimers AB and B3 show similar spectral features as the BB dimer throughout the entire measured IR range which is indicative of a beta-sheet structure with a parallel orientation. The linear conformation of at least one of the monomeric units in the dimer assist the beta-sheet formation. Concluding, the observed and assigned monomeric peptide conformers are retained upon dimerization, and thus direct their final structural arrangement. Currently, higher order peptide aggregates are studied to evaluate how these conclusions can be extrapolated.

Conflicts of interest

There are no conflicts to declare.

Acknowledgements

We gratefully acknowledge the Nederlandse Organisatie voor Wetenschappelijk Onderzoek (NWO) for the support of the FELIX Laboratory. Calculations were carried out at the SurfSARA Cartesius cluster under NWO Rekentijd contract 16327.

Notes and references

1. F. Chiti and C. M. Dobson, *Annu. Rev. Biochem.*, 2006, **75**, 333-366.
2. C. M. Dobson, *Nature*, 2003, **426**, 884-890.
3. T. P. Knowles, M. Vendruscolo and C. M. Dobson, *Nat. Rev. Mol. Cell. Biol.*, 2014, **15**, 384-396.
4. A. E. Ashcroft, *J. Am. Soc. Mass. Spectrom.*, 2010, **21**, 1087-1096.
5. D. Eisenberg, R. Nelson, M. R. Sawaya, M. Balbirnie, S. Sambashivan, M. I. Ivanova, A. O. Madsen and C. Riekel, *Acc. Chem. Res.*, 2006, **39**, 568-575.
6. K. A. Dill and J. L. MacCallum, *Science*, 2012, **338**, 1042-1046.
7. J. Greenwald and R. Riek, *Structure*, 2010, **18**, 1244-1260.
8. L. E. Buchanan, E. B. Dunkelberger, H. Q. Tran, P. N. Cheng, C. C. Chiu, P. Cao, D. P. Raleigh, J. J. de Pablo, J. S. Nowick and M. T. Zanni, *Proc. Natl. Acad. Sci. U.S.A.*, 2013, **110**, 19285-19290.
9. A. Laganowsky, C. Liu, M. R. Sawaya, J. P. Whitelegge, J. Park, M. L. Zhao, A. Pensalfini, A. B. Soriaga, M. Landau, P. K. Teng, D. Cascio, C. Glabe and D. Eisenberg, *Science*, 2012, **335**, 1228-1231.
10. P. Neudecker, P. Robustelli, A. Cavalli, P. Walsh, P. Lundstrom, A. Zarrine-Afsar, S. Sharpe, M. Vendruscolo and L. E. Kay, *Science*, 2012, **336**, 362-366.
11. A. Bleem and V. Daggett, *Biotechnol. Bioeng.*, 2017, **114**, 7-20.
12. C. Seuring, K. Ayyer, E. Filippaki, M. Barthelmess, J. N. Longchamp, P. Ringler, T. Pardini, D. H. Wojtas, M. A. Coleman, K. Dorner, S. Fuglerud, G. Hammarin, B. Habenstein, A. E. Langkilde, A. Loquet, A. Meents, R. Riek, H. Stahlberg, S. Boutet, M. S. Hunter, J. Koglin, M. N. Liang,

H. M. Ginn, R. P. Millane, M. Frank, A. Barty and H. N. Chapman, *Nat. Comm.*, 2018, **9**.
13. Z. A. Levine and J. E. Shea, *Curr. Opin. Struct. Biol.*, 2017, **43**, 95-103.
14. C. Wasmer, A. Lange, H. Van Melckebeke, A. B. Siemer, R. Riek and B. H. Meier, *Science*, 2008, **319**, 1523-1526.
15. P. I. Haris, *Biochim. Biophys. Acta Biomembranes*, 2013, **1828**, 2265-2271.
16. S. L. Bernstein, N. F. Dupuis, N. D. Lazo, T. Wyttenbach, M. M. Condron, G. Bitan, D. B. Teplow, J. E. Shea, B. T. Ruotolo, C. V. Robinson and M. T. Bowers, *Nat. Chem.*, 2009, **1**, 326-331.
17. C. Bleiholder, N. F. Dupuis, T. Wyttenbach and M. T. Bowers, *Nat. Chem.*, 2011, **3**, 172-177.
18. W. Hoffmann, K. Folmert, J. Moschner, X. Huang, H. von Berlepsch, B. Koksch, M. T. Bowers, G. von Helden and K. Pagel, *J. Am. Chem. Soc.*, 2018, **140**, 244-249.
19. J. Seo, W. Hoffmann, S. Warnke, X. Huang, S. Gewinner, W. Schollkopf, M. T. Bowers, G. von Helden and K. Pagel, *Nat. Chem.*, 2017, **9**, 39-44.
20. M. Z. Kamrath and T. R. Rizzo, *Acc. Chem. Res.*, 2018, **51**, 1487-1495.
21. H. Elferink, M. E. Severijnen, J. Martens, R. A. Mensink, G. Berden, J. Oomens, F. Rutjes, A. M. Rijs and T. J. Boltje, *J. Am. Chem. Soc.*, 2018, **140**, 6034-6038.
22. J. Ujma, V. Kopysov, N. S. Nagornova, L. G. Migas, M. G. Lizio, E. W. Blanch, C. MacPhee, O. V. Boyarkin and P. E. Barran, *Angew. Chem. Int. Ed.*, 2018, **57**, 213-217.
23. N. Borho, M. A. Suhm, K. Le Barbu-Debus and A. Zehnacker, *Phys. Chem. Chem. Phys.*, 2006, **8**, 4449-4460.
24. K. Schwing and M. Gerhards, *Int. Rev. Phys. Chem.*, 2016, **35**, 569-677.
25. E. Gloaguen and M. Mons, in *Gas-Phase Ir Spectroscopy and Structure of Biological Molecules*, eds. A. M. Rijs and J. Oomens, 2015, vol. 364, pp. 225-270.
26. S. Habka, W. Y. Sohn, V. Vaquero-Vara, M. Geleoc, B. Tardivel, V. Brenner, E. Gloaguen and M. Mons, *Phys. Chem. Chem. Phys.*, 2018, **20**, 3411-3423.
27. M. Gerhards and C. Unterberg, *Phys. Chem. Chem. Phys.*, 2002, **4**, 1760-1765.
28. M. Gerhards, C. Unterberg and A. Gerlach, *Phys. Chem. Chem. Phys.*, 2002, **4**, 5563-5565.
29. M. Gerhards, C. Unterberg, A. Gerlach and A. Jansen, *Phys. Chem. Chem. Phys.*, 2004, **6**, 2682-2690.
30. A. Gerlach, C. Unterberg, H. Fricke and M. Gerhards, *Mol. Phys.*, 2005, **103**, 1521-1529.
31. T. D. Vaden, S. A. N. Gowers and L. C. Snoek, *J. Am. Chem. Soc.*, 2009, **131**, 2472-2474.
32. D. J. Bakker, A. Dey, D. P. Tabor, Q. Ong, J. Mahe, M. P. Gaigeot, E. L. Sibert and A. M. Rijs, *Phys. Chem. Chem. Phys.*, 2017, **19**, 20343-20356.
33. M. Cirtog, A. M. Rijs, Y. Loquais, V. Brenner, B. Tardivel, E. Gloaguen and M. Mons, *J. Phys. Chem. Lett.*, 2012, **3**, 3307-3311.
34. A. M. Rijs, N. Sandig, M. N. Blom, J. Oomens, J. S. Hannam, D. A. Leigh, F. Zerbetto and W. J. Buma, *Ang. Chem. Int. Ed.*, 2010, **49**, 3896-3900.
35. H. Zhu, M. Blom, I. Compagnon, A. M. Rijs, S. Roy, G. von Helden and B. Schmidt, *Phys. Chem. Chem. Phys.*, 2010, **12**, 3415-3425.
36. Y. J. Hu and E. R. Bernstein, *J. Phys. Chem. A*, 2009, **113**, 8454-8461.
37. J. J. Lee, M. Albrecht, C. A. Rice and M. A. Suhm, *J. Phys. Chem. A*, 2013, **117**, 7050-7063.
38. S. Bakels, S. B. A. Porskamp and A. M. Rijs, *To be published*, 2019.
39. A. M. Rijs, E. R. Kay, D. A. Leigh and W. J. Buma, *J. Phys. Chem. A*, 2011, **115**, 9669-9675.
40. A. M. Rijs and J. Oomens, *Top. Curr. Chem.*, 2015, **364**, 1-42.
41. P. M. Johnson and C. E. Otis, *Annu. Rev. Phys. Chem.*, 1981, **32**, 139-157.
42. D. Oepts, A. F. G. van der Meer and P. W. van Amersfoort, *Infrared Phys. Technol.*, 1995, **36**, 297-308.
43. D. A. Case, T. A. Darden, T. E. Cheatham III, C. L. Simmerlin, J. Wang, R. E. Duke, R. Luo, R. C. Walker, W. Zhang, K. M. Merz, B. Roberts, S. Hayik, A. Roitberg, G. Seabra, J. Swails, A. W. Götz, I. Kolossváry, K. F. Wong, F. Paesani, J. Vanicek, R. M. Wolf, J. Liu, X. Wu, S. R. Brozell, T. Steinbrecher, H. Gohlke, Q. Cai, X. Ye, J. Wang, M.-J. Hsieh, G. Cui, D. R. Roe, D. H. Mathews, M. G. Seetin, R. Salomon-Ferer, C. Sagui, V. Babin, T. Luchko, S. Gusarov, A. Kovalenko and P. A. Kollman, *AMBER 12*, 2012.
44. S. Grimme, J. Antony, S. Ehrlich and H. Krieg, *J. Chem. Phys.*, 2010, **132**.
45. M. J. Frisch, G. W. Trucks, H. B. Schlegel, G. E. Scuseria, M. A. Robb, J. R. Cheeseman, G. Scalmani, V. Barone, G. A. Petersson, H. Nakatsuji, X. Li, M. Caricato, A. Marenich, J. Bloino, B. G. Janesko, R. Gomperts, B. Mennucci, H. P. Hratchian, J. V. Ortiz, A. F. Izmaylov, J. L. Sonnenberg, D. Williams-Young, F. Ding, F. Lipparini, F. Egidi, J. Goings, B. Peng, A. Petrone, T. Henderson, D. Ranasinghe, V. G. Zakrzewski, J. Gao, N. Rega, G. Zheng, W. Liang, M. Hada, M. Ehara, K. Toyota, R. Fukuda, J. Hasegawa, M. Ishida, T. Nakajima, Y. Honda, O. Kitao, H. Nakai, T. Vreven, K. Throssell, J. A. J. Montgomery, J. E. Peralta, F. Ogliaro, M. Bearpark, J. J. Heyd, E. Brothers, K. N. Kudin, V. N. Staroverov, T. Keith, R. Kobayashi, J. Normand, K. Raghavachari, A. Rendell, J. C. Burant, S. S. Iyengar, J. Tomasi, M. Cossi, J. M. Millam, M. Klene, C. Adamo, R. Cammi, J. W. Ochterski, R. L. Martin, K. Morokuma, O. Farkas, J. B. Foresman and D. J. Fox, *Gaussian 09, Revision E.01*, 2016.
46. A. M. Rijs, I. Compagnon, J. Oomens, J. S. Hannam, D. A. Leigh and W. J. Buma, *J. Am. Chem. Soc.*, 2009, **131**, 2428-2429.
47. E. Gloaguen, B. de Courcy, J. P. Piquemal, J. Pilme, O. Parisel, R. Pollet, H. S. Biswal, F. Piuzzi, B. Tardivel, M. Broquier and M. Mons, *J. Am. Chem. Soc.*, 2010, **132**, 11860-11863.
48. L. Voronina and T. R. Rizzo, *Phys. Chem. Chem. Phys.*, 2015, **17**, 25828-25836.
49. J. A. Silveira, K. L. Fort, D. Kim, K. A. Servage, N. A. Pierson, D. E. Clemmer and D. H. Russell, *J. Am. Chem. Soc.*, 2013, **135**, 19147-19153.
50. V. Yatsyna, D. J. Bakker, P. Salen, R. Feifel, A. M. Rijs and V. Zhaunerchyk, *Phys. Rev. Lett.*, 2016, **117**.